Supporting Information

Atomic-Layer-Deposited Pd/Cu_2O/Cu Heterojunction as High-Efficiency Formate Catalysts and Boosting Aqueous Zn-CO_2 Batteries

Jia Xu, Li Tao, Yue Zhang, Evan J. Hansen, Robert Godin and Jian Liu**

*Corresponding authors.

E-mail: jian.liu@ubc.ca (J. Liu); robert.godin@ubc.ca (R. Godin)

1. Experimental Section

1.1 Materials

All chemical reagents were used directly without further treatment. Copper (II) Chloride ($CuCl_2$; CAS No: 7447-39-4) and sodium hydroxide (NaOH; CAS No: 1310-73-2) were purchased from Ward's Science. Ascorbic acid ($C_6H_8O_6$; CAS No: 50-81-7) was purchased from VWR. Palladium hexafluoroacetylacetonate ($Pd(hfac)_2$; CAS No: 64916-48-9) was acquired from STREM Chemicals, INC. Potassium bicarbonate ($KHCO_3$; CAS No: 5970-45-6) was acquired from Thermo Scientific Chemicals. Ethanol (EtOH, ≥99.7%) and isopropanol (*i*-PrOH, ≥99.7%) were sourced from Alfa Aesar.

1.2 Synthesis of Cu_2O nanocubes

Cu_2O nanocubes were synthesized by slight modification of previous methods.[26] Specifically, $CuCl_2$ aqueous solution (0.1 mol L^{-1}; 10 mL) was added dropwise to 90 mL of deionized water (DIW) and subsequently heated in a water bath at 55 °C. Then, NaOH aqueous solution (2 mol L^{-1}; 10 mL) was added to the above aqueous solution and stirred for 0.5 h. Ascorbic acid solution (0.6 mol L^{-1}; 10 mL) was added dropwise, stirring at 55 °C for an additional 3 h. The obtained orange precipitate was collected by centrifugation and rinsed at least three times with DIW and ethanol. Finally, the Cu_2O nanocube powder was dried in a vacuum drying box at room temperature.

1.3 Preparation of Cu_2O/Cu and Pd–Cu_2O/Cu catalyst

Pd deposition on Cu_2O nanocubes was performed at 150°C with an alternating supply of $Pd(hfac)_2$ and plasma H_2 into a plasma-enhanced atomic layer deposition (ALD) reactor (GEMStar™ XT Atomic Layer Deposition System). The Pd layers were deposited onto the Cu_2O nanocubes by adjusting the ALD cycle count to 100, which were named Cu_2O@Pd-100.

To prepare the catalyst ink, 10 mg of Cu_2O/Pd-100 electrocatalyst was ultrasonically dispersed for 1 h into 500 µL of isopropanol containing a 0.05 wt% Nafion™ solution and 60 µL of distilled water. The resulting suspension was drop-casted onto a gas diffusion electrode (GDE) to achieve a catalyst loading of 0.5 mg cm^{-2}. The Pd–Cu_2O/Cu catalyst was then obtained by electrochemical reduction of the Cu_2O@Pd-100 on a GDE in 0.5 M $KHCO_3$ electrolyte at −0.5 V *vs.* RHE for 10 min. For comparison, the Cu_2O/Cu catalyst was prepared using an identical electrochemical reduction procedure with pristine Cu_2O on a GDE.

1.4 Characterization Methods

Raman spectroscopy was performed using a Bruker SENTERRA II spectrometer with a 532 nm laser operating at 25 mW. X-ray diffraction (XRD) measurements were performed using Cu-Kα radiation (λ = 1.5418 Å) at a scanning rate of 5° min^{-1}. Scanning electron microscopy (SEM, Tescan Mira 3 XMU) and transmission electron microscopy (TEM, Tecnai F20) and high-angle annular dark field TEM (HAADF-TEM, Tecnai F20) were employed to investigate the morphology and microstructure of the samples. X-ray photoelectron spectroscopy (XPS) analyses were conducted on a PHI 5700 ESCA system. Inductively coupled plasma optical emission spectroscopy (ICP-AES, ThermoFisher iCAP 6000) was run out to test the Pd element content.

1.5 Electrochemical characterization

Electrochemical measurements were carried out using a Biologic SP-150 electrochemical workstation. A three-electrode, Platinum mesh (CE), Ag/AgCl (RE) and GDE modified with electrocatalysts (WE) were applied with a 0.5 M $KHCO_3$ solution saturated with CO_2 (pH = 7.5). The H cell comprised two glass compartments connected by a metal clamp. The anolyte and catholyte were separated using a Nafion™ membrane (117 Nafion™) during the experimentation. The WE consisted of a gas diffusion electrode (GDE, Freudenberg H23C3, Model 1590044, Fuel Cell Store) modified with an electrocatalyst ink suspension. All measurements were performed in 0.5 M $KHCO_3$ electrolyte. A mass flow controller (ALICAT Scientific) was employed to regulate the CO_2 gas flow at 10 sccm. The electrochemical double-layer capacitance (C_{dl}) was determined from cyclic voltammetry (CV) at various scan rates.

Gaseous products were analyzed using the H-type cell coupled with a gas chromatograph (Thermo Scientific, Trace 1300 series) equipped with an automated injection system. The GC was equipped with a pulsed discharge detector (PDD) and operated with an oven temperature ramp from 50 to 250 °C over 30 min. Liquid products in the electrolyte were analyzed *ex situ* by nuclear magnetic resonance (NMR) spectroscopy (Bruker AVII 600 MHz) using ^1H spectra with water suppression (Watergate W5 pulse sequence, 256 scans) after 20 min of chronoamperometry. For NMR analysis, 686 µL of electrolyte (from the total 60 mL)

was mixed with 34 µL of d_6-dimethyl sulfoxide (DMSO, internal standard, Sigma-Aldrich, CAS: 2206-27-1) and 80 µL of D_2O.

Faradaic efficiency (FE) for gaseous products was calculated according to Equation (1):

$$FE\% = V \times \frac{Z_i C_i F}{i} \times 100 \quad (1)$$

Where V is the volume of gas leaving the cell, Z_i is the number of electrons transferred for the formation of the product, C_i is the concentration of the corresponding gas product, F is the Faraday constant, and i is the applied current.

Faradaic efficiency (FE) for liquid products was determined using Equation (2):

$$FE\% = V_{total} \times \frac{Z_i C_i F}{C_{total}} \times 100 \quad (2)$$

Where V_{total} is the total volume of the collected electrolyte sample, C_{total} is the total charge passed during electrolysis, Z_i is the number of electrons required to produce one molecule of the product, C_i is the concentration of the product determined from the NMR integration data, and F is the faraday constant.

The concentration of liquid products (C_i) was calculated according to Equation (3):

$$C_i = \frac{I_i}{I_{std}} \times \frac{n_{std}}{n_i} C_{std} \quad (3)$$

Where I_i and I_{std} are the NMR integration areas of the product and the internal standard (DMSO), respectively, and n_i and n_{std} represent the number of protons contributing to the NMR signal of the product and the standard, respectively, C_{std} is the known concentration of the internal standard, used to calculate the single product concentration.

1.6 Zn-CO_2 battery measurement

A cell arrangement consisting of two chambers separated by a Nafion™ membrane (111 Nafion™) was used to construct the Zn-CO_2 battery as shown in the inset of **Figure 5b**. The electrocatalysts were drop-cast onto GDE with an areal loading of 0.5 mg cm^{-2} and a cathode

area of 1 cm^2. The anode using Zn foil was first cleaned with isopropanol. The anolyte chamber was filled with a 1.0 M KOH + 0.02 M $Zn(CH_3CO_2)_2$ solution, the catholyte chamber was filled with a 0.5 M $KHCO_3$ solution, and the gas chamber on the cathode side was continuously purged with CO_2 at 10 sccm. The CO_2 battery performance was tested using galvanostatic charge and discharge testing with a Biologic SP-150 workstation. The charge and discharge cycles were each set to 20 mins (total 40 mins per cycle), and linear sweep voltammetry (LSV) was performed at 10 mV s^{-1} to produce the polarization curves.

1.7 Computational details

All calculations were performed within the framework of density functional theory (DFT) using the projector augmented plane-wave (PAW) method, as implemented in the Vienna Ab Initio Simulation Package (VASP).[1] The generalized gradient approximation (GGA) proposed by Perdew, Burke, and Ernzerhof (PBE) was adopted for the exchange-correlation potential.[2] Long-range van der Waals interactions were described using the DFT-D3 approach.[3] A plane-wave cutoff energy of 400 eV was employed. A vacuum layer of 20 Å was added perpendicular to the sheet to prevent artificial interactions between periodic images. Brillouin zone integration was performed using a 1 × 1 × 1 k-point mesh. All structures were relaxed until the residual forces on the atoms decreased to less than 0.05 eV/Å.

References

1) Kresse, G.; Joubert, D. From ultrasoft pseudopotentials to the projector augmented-wave method. Physical Review B 1999, 59, 1758-177.
2) Perdew, J. P.; Burke, K.; Ernzerhof, M. Generalized gradient approximation made simple. Physical Review Letters 1996, 77, 3865-3868.
3) Grimme S, Antony J, Ehrlich S and Krieg H 2010 A consistent and accurate ab initio parametrization of density functional dispersion correction (DFT-D) for the 94 elements H-Pu Journal of Chemical Physics 2010, 132, 154104.

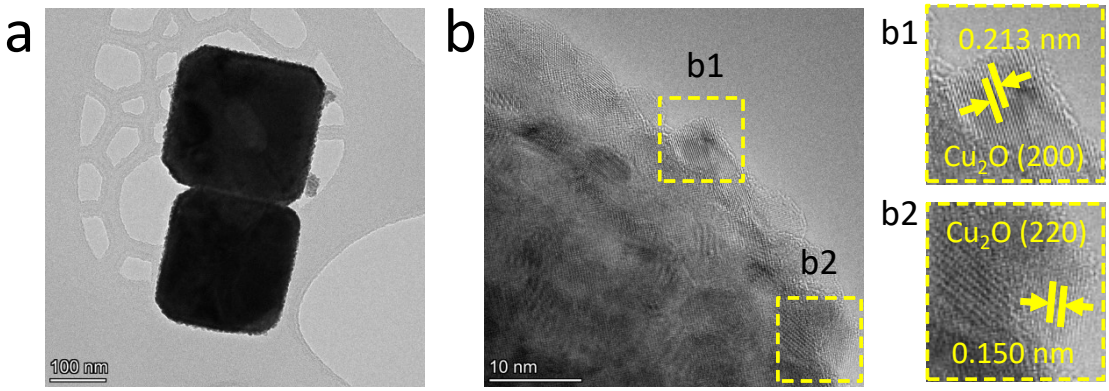

Figure S1 (a, b) TEM images of Cu_2O. (b1, b2) Enlarged TEM images of Cu_2O.

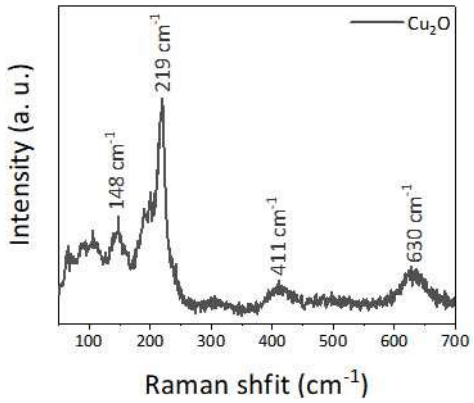

Figure S2 Raman spectrum of Cu_2O.

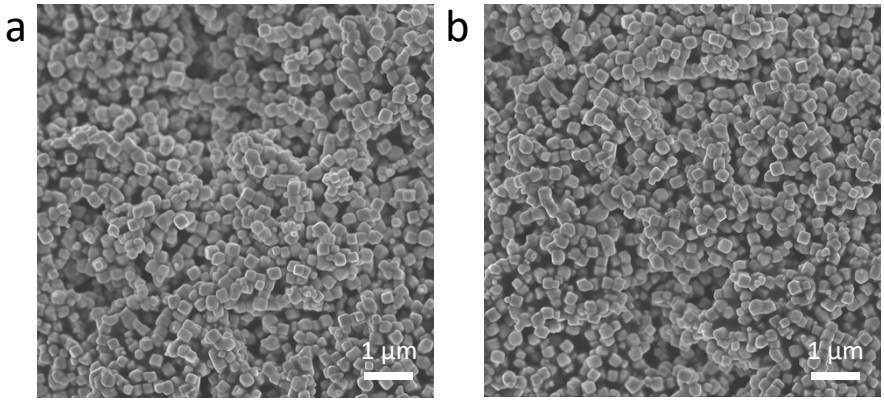

Figure S3 SEM images of Cu_2O@Pd-100.

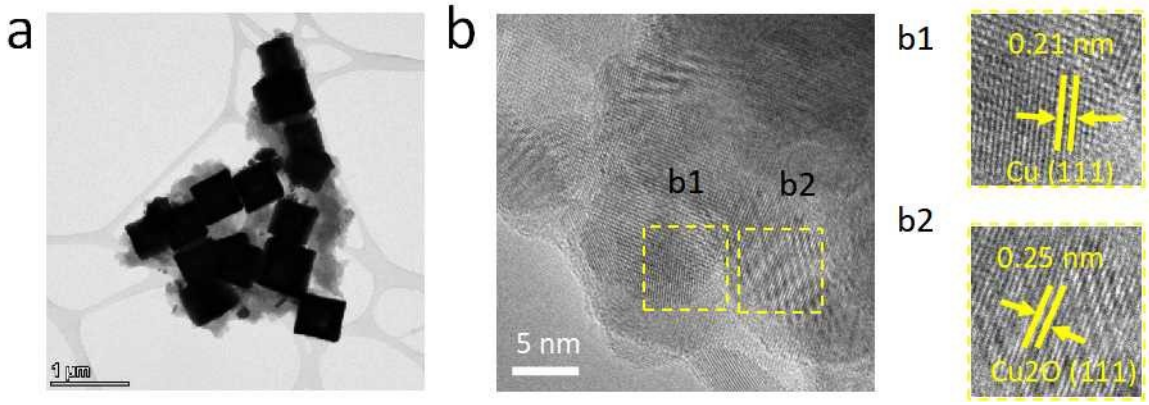

Figure S4 (a) TEM and (b) HR-TEM images of Cu_2O/Cu. (b1, b2) Enlarged TEM images of Cu_2O/Cu.

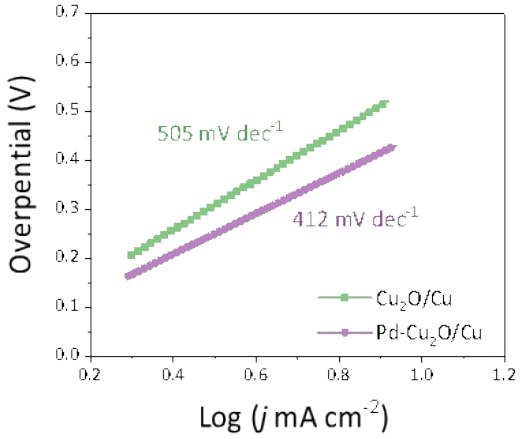

Figure S5 Tafel slops of Cu_2O/Cu and Pd–$C_{u2}O$/Cu.

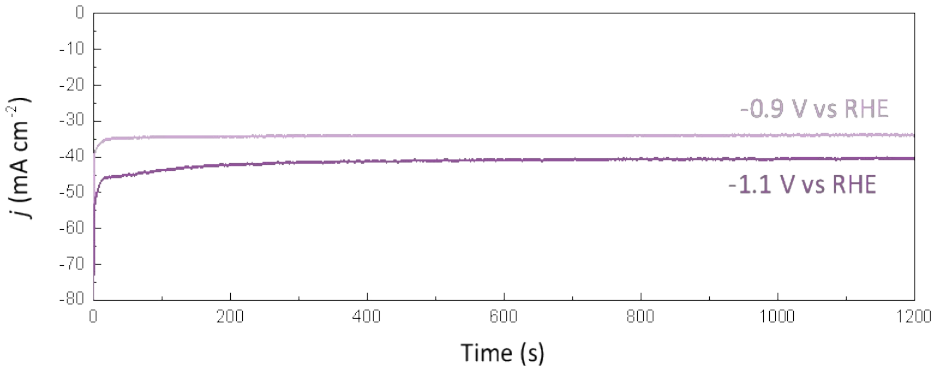

Figure S6 The chronoamperometry (CA) curves of Pd–Cu_2O/Cu at -0.9 V and -1.1 V (vs RHE).

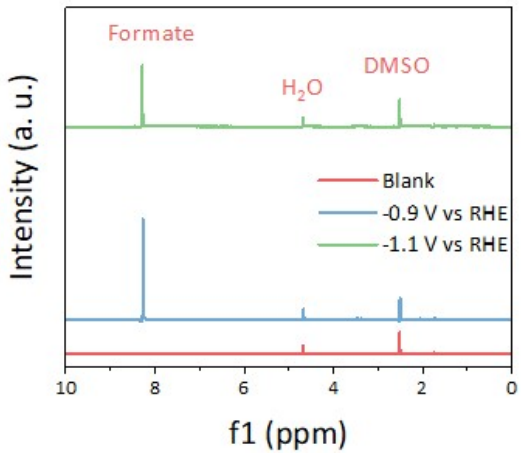

Figure S7 ^{1}H NMR spectra of Pd–Cu_2O/Cu.

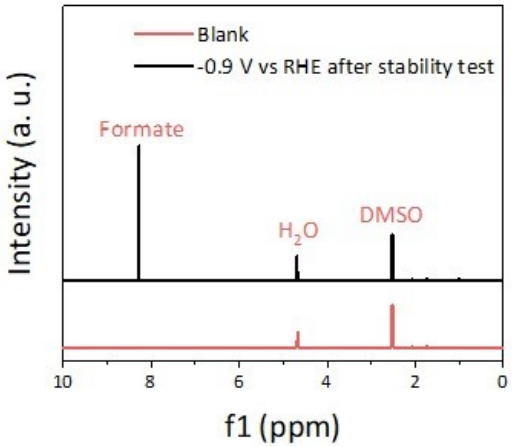

Figure S8 ^{1}H NMR spectra of Pd–Cu_2O/Cu after stability test at -0.9 V (vs RHE) for 12h.

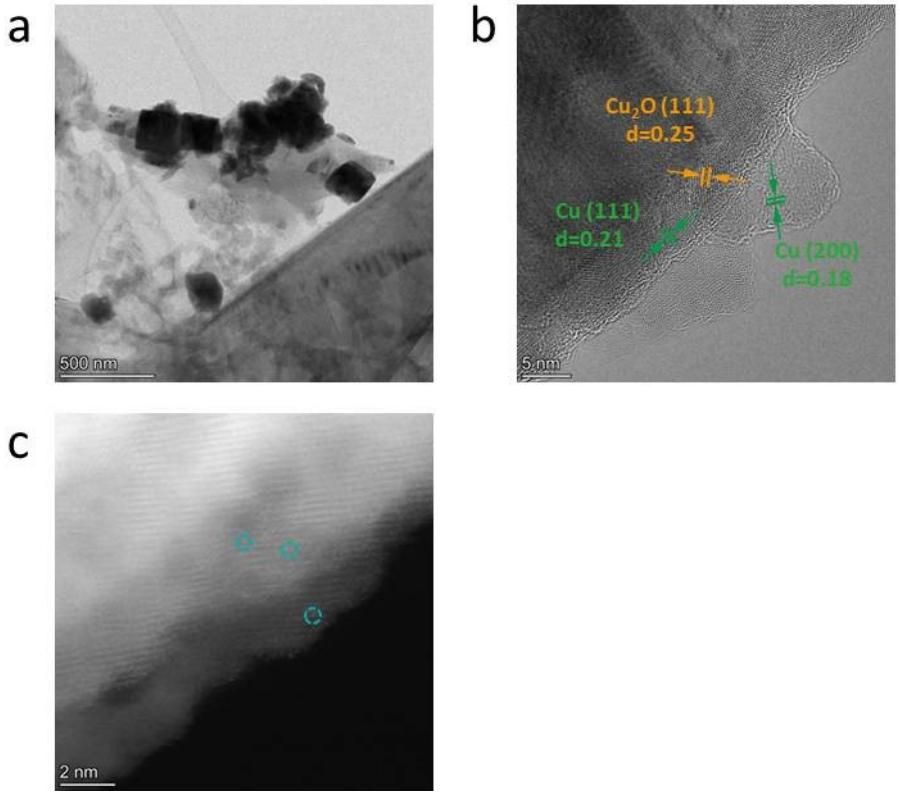

Figure S9 (a) TEM, (b) HRTEM and (c) AC-HAADF-STEM images of Pd–Cu_2O/Cu after stability test at -0.9 V (vs RHE) for 12h.

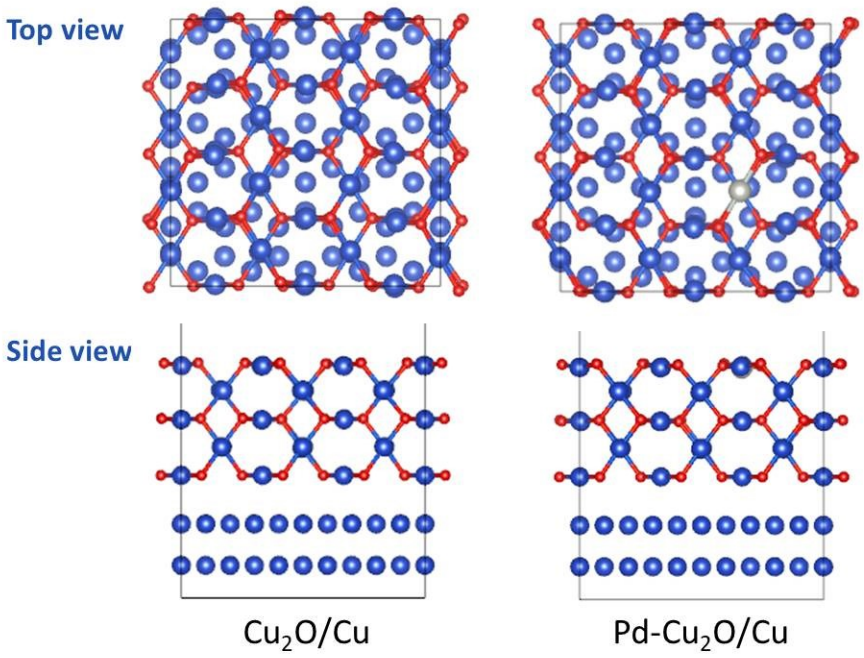

Figure S10 Top view and side view of Cu_2O/Cu and Pd–Cu_2O/Cu models.

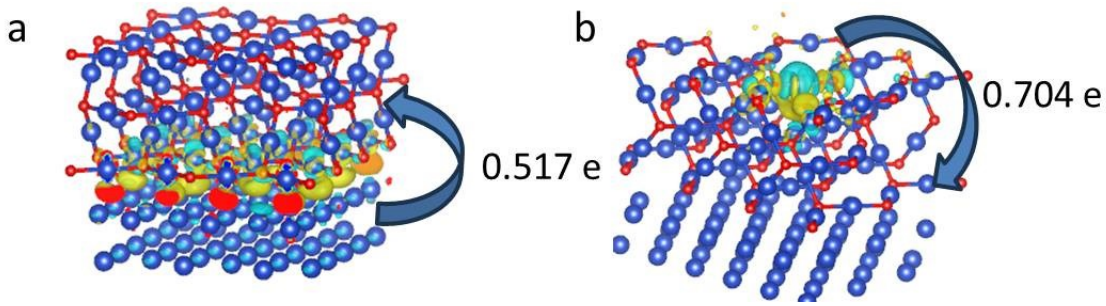

Figure S11 Differential charge density of (a) Cu_2O/Cu and (b) Pd–Cu_2O/Cu models.

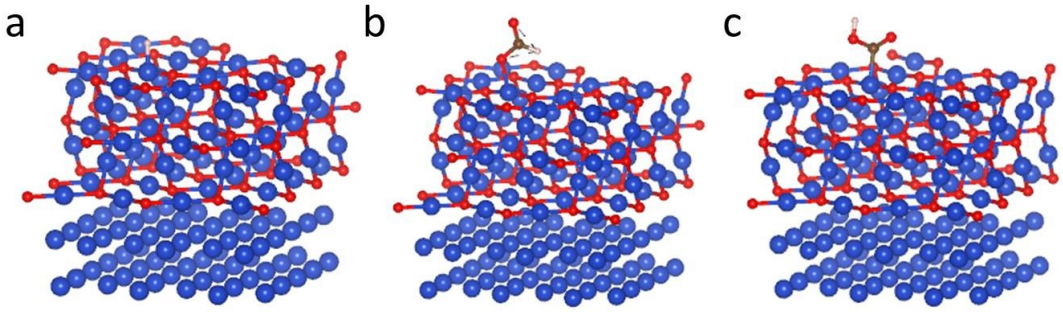

Figure S12 Schematic diagram of (a) *H, (b) *OCHO and (c) *COOH adsorbed on Cu_2O/Cu.

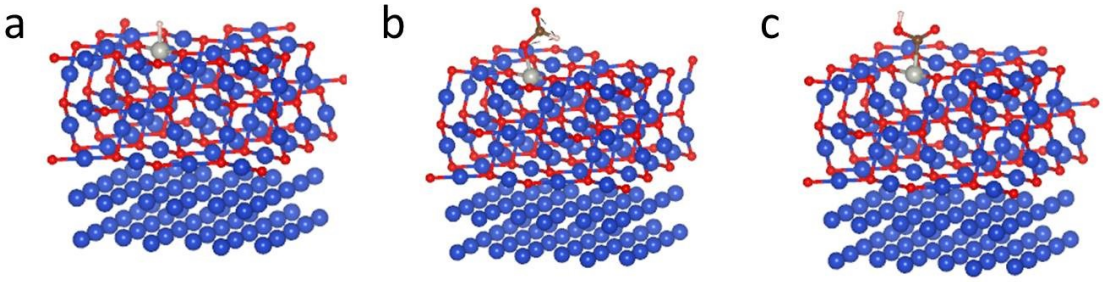

Figure S13 Schematic diagram of (a) *H, (b) *OCHO and (c) *COOH adsorbed on Pd-Cu_2O/Cu.

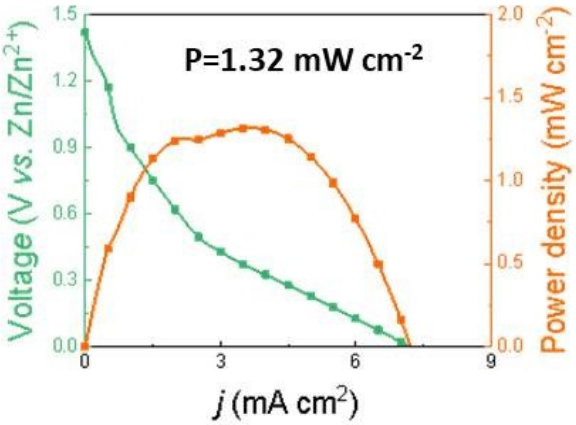

Figure S14 Discharge curves and power density of ZCBs with Cu_2O/Cu as the cathode.

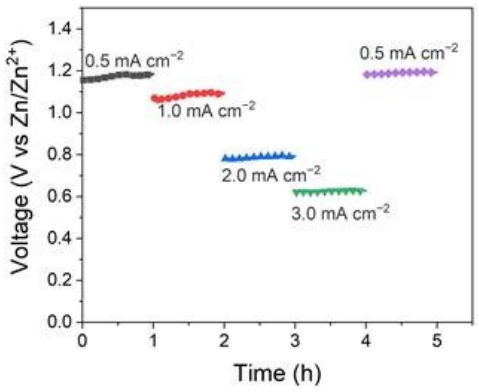

Figure S15 Galvanostatic discharge curves at different current densities.

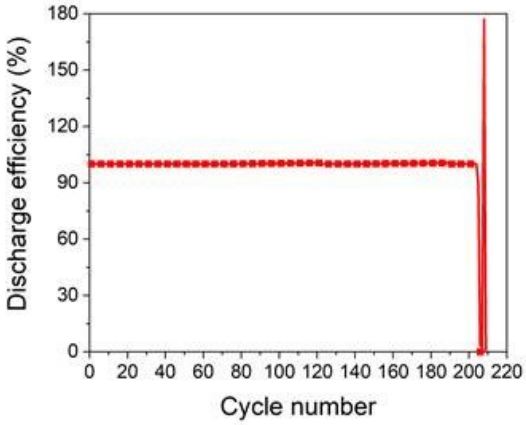

Figure S16 Discharge efficiency of ZCBs at 0.5 mA cm^{-2}.

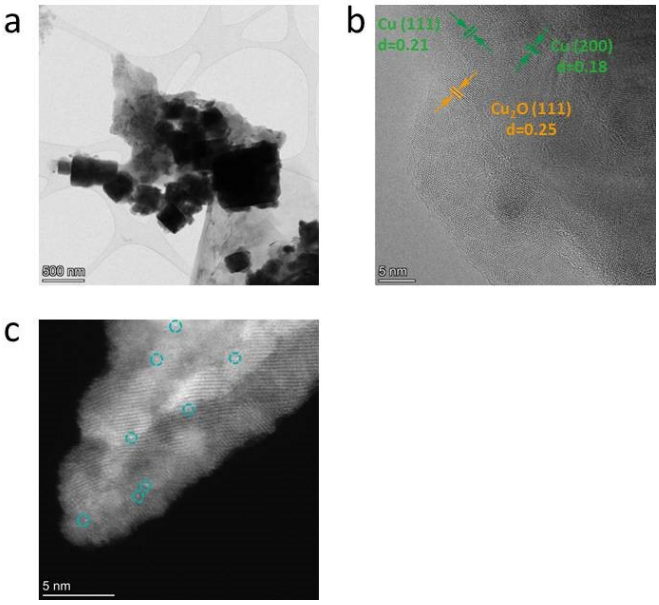

Figure S17 (a) TEM, (b) HRTEM and (c) AC-HAADF-STEM images of Pd-Cu_2O/Cu as the cathode after ZCBs cycling.

Tables S1. Comparison of the performance of the presented Pd–Cu_2O/Cu catalyst with several recently reported CO_2-to-HCOOH reduction catalysts.

Catalysts	Electrolyte	Products	Voltage (V vs RHE)	FE (%)	$j_{formate}$ (mA cm^{-2})	Stability (h)	Ref.
Pd–Cu_2O/Cu	**0.5 M $KHCO_3$**	**Formate**	**-0.9**	**61.1%**	**~-24**	**12**	**This work**
Cu_2O@Cu	0.5 M $KHCO_3$	Formate	-0.6	~50%	~-20	-	Energy Environ. Sci. 2024, 17, 6779-6786.
Pd_{40}/Cu_2O-Cu	0.5 M $KHCO_3$	Formate	-0.25	92%	-4.5	3	ChemSusChem 2019, 12, 4471-4479.
CuS_x-Ag/Cu	0.1 M $KHCO_3$	Formate	-0.6	87%	-9.6	65	ACS Catal. 2022, 12, 21, 13174–13185.
Sn-CF1000	0.1 M $KHCO_3$	Formate	-0.69	62%	-11	24	Adv. Energy Mater. 2018, 8, 1702524.
Densed tip Sn	1.0 M $KHCO_3$	Formate	-0.76	50%	~62.5	72	J. Mater. Chem. A 2020, 8, 9032-9038.
SnO_2 NPs	1.0 M KOH	Formate	-0.95	46%	147	-	J. Mater. Chem. A 2018, 6, 10313-10319.
Pd–B/C	0.1 M $KHCO_3$	Formate	-0.5	70%	~3.98	5	J. Am. Chem. Soc. 2018, 140, 8, 2880–2889.
Sn/SnO_x thin film	0.5 M $NaHCO_3$	Formate	-0.7	70%	1.6	12	J. Am. Chem. Soc. 2012, 134, 1986.
Sn gas diffusion electrode	0.1 M $NaHCO_3$	Formate	-1.2	64%	-	2	J. Mater. Chem. A 2014, 2, 1647.
Pd/hNCNCs	0.1 M $KHCO_3$	Formate	-0.27	99.8%	~2	8	Adv. Mater. 2020, 32 , e2000992.

Tables S2. Comparison of Zn–CO_2 battery performance.

Catalysts	Catholyte	Discharge products	OCV (V)	Power density (mW cm^{-2})	Stability (h)	Ref.
Pd–Cu_2O/Cu	**0.5 M $KHCO_3$**	**Formate**	**1.41**	**2.54**	**135**	**This work**
Bi-D	2 M $KHCO_3$ + 0.02 M $HCOO^-$	Formate	1.3	1.2	22	Chem. Commun. 2022, 58, 3621.
Cu–N_2/GN	0.5 M $KHCO_3$	CO	-	0.62	40	Adv. Funct. Mater. 2020, 30, 1907658.
BiC/HCS	0.1 M $KHCO_3$	Formate	0.94	7.2 ± 0.5	10	Applied Catalysis B: Environmental 2022, 307, 121145.
BiPd	0.1 M $KHCO_3$ + 0.1 M HCOONa	Formate	1.2	0.42	45	ACS Appl. Nano Mater. 2022, 5, 12387−12394.
Ir@Au	0.8 M $KHCO_3$	CO	0.71	-	30	Adv. Mater. 2019, 31, 1807807.
Fe_1NC/S_1-1000	0.8 M $KHCO_3$	CO	0.73	0.6	25	Adv. Mater. 2020, 32, 2002430.
NOMC	0.8 M $KHCO_3$	CO	0.9	0.71	100	Small Methods 2021, 2001039.
Pd deposited carbon paper	0.1 M NaCl + 0.1 M HCOONa	HCOOH	0.9	-	30	Angew. Chem. Int. Ed. 2018, 57, 16996-17001.
FeN_5@DNC	0.5 M $KHCO_3$	CO	-	0.6	24	Angew. Chem. Int. Ed. 2024, 63 e202406030.
CoPc@DNHCS-8	0.8 M $KHCO_3$	CO	-	1.02	40	Adv. Funct. Mater. 2022, 32, 2110649.
CuNi-DSACs	1.0 M $KHCO_3$	CO	-	1.04	46	Angew. Chem. Int. Ed. 2024, e202415223.
PNCB	2 M $KHCO_3$ + 0.2 M HCOOH	HCOOH	1.1	1.43	20	Nano Energy 2022, 92, 106780.
s-SnLi	6 M KOH + 0.02 M $Zn(Ac)_2$	HCOOH	0.14	1.24	85	Angew. Chem. Int. Ed. 2021, 60, 25741-25745.